Cancer Nanotechnology

# Synergistic co-administration of docetaxel and curcumin to chemoresistant cancer cells using PEGylated and RIPL peptide-conjugated nanostructured lipid carriers

Chang Hyun Kim[1], Byoung Deok Kim[1], Tae Hwa Lee[1], Hyeon Kyun Kim[1], Min Jeong Lyu[1], Young In Yoon[1], Yoon Tae Goo[1], Myung Joo Kang[2], Sangkil Lee[3] and Young Wook Choi[1*]

*Correspondence:
ywchoi@cau.ac.kr

[1] College of Pharmacy, Chung-Ang University, 84 Heuksuk-ro, Dongjak-gu, Seoul 06974, Republic of Korea
[2] College of Pharmacy, Dankook University, 119 Dandae-ro, Dongnam-gu, Cheonan, Chungnam 31116, Republic of Korea
[3] College of Pharmacy, Keimyung University, 1095 Dalgubeol-daero, Daegu 42601, Republic of Korea
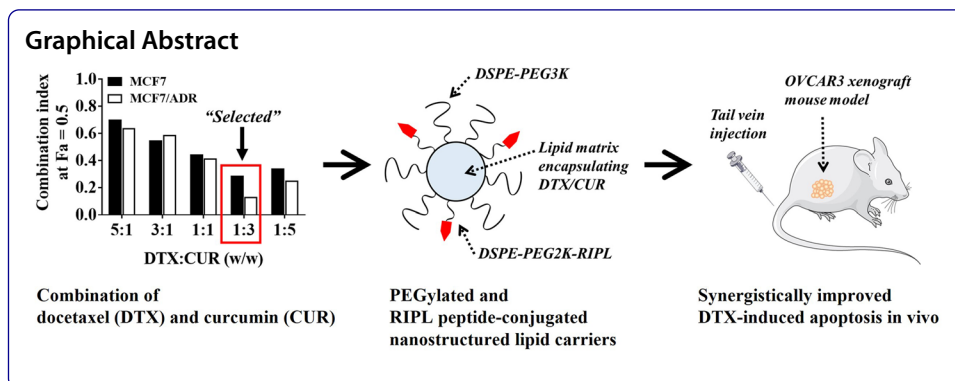
## Abstract

**Background:** A targeted co-administration system of docetaxel (DTX) and curcumin (CUR) using a PEG-modified RIPL peptide (IPLVVPLRRRRRRRRC)-conjugated nanostructured lipid carrier (P/R-NLC) was constructed to exert synergistic anticancer effects against chemoresistant breast cancer.

**Results:** DTX- or CUR-loaded NLCs and P/R-NLCs were prepared using the solvent emulsification–evaporation method. NLCs showed homogeneous spherical morphology with nano-sized dispersion (< 210 nm) with zeta potential varying from − 16.4 to − 19.9 mV. DTX or CUR was successfully encapsulated in the NLCs: encapsulation efficiency (> 95%); drug loading (8 − 18%). All NLC formulations were stable for 4 weeks under the storage conditions at 4 °C. Drug release was diffusion-controlled, revealing the best fit to the Higuchi equation. DTX- or CUR-loaded formulations showed dose-dependent cytotoxicity. The DTX/CUR combination (1:3 w/w) in P/R-NLC formulations exhibited the strongest synergism in both MCF7 and MCF7/ADR cells with combination index values of 0.286 and 0.130, respectively. Co-treatment with DTX- or CUR-P/R-NLCs increased apoptosis in both cell lines exhibited the superior synergistic inhibitory effect on MCF7/ADR three-dimensional spheroids. Finally, in OVCAR3-xenografted mouse models, co-treatment with DTX- or CUR-loaded P/R-NLCs significantly suppressed tumor growth compared to the other treatment groups.

**Conclusions:** Co-administration of DTX/CUR (1:3 w/w) using P/R-NLCs induced a synergistic effect against chemoresistant cancer cells.

**Keywords:** Synergistic, Anticancer, Breast cancer, Nano-lipid carrier, Drug evaluation, Growth inhibition

**Graphical Abstract**

Combination of docetaxel (DTX) and curcumin (CUR)

PEGylated and RIPL peptide-conjugated nanostructured lipid carriers

Synergistically improved DTX-induced apoptosis in vivo

## Background

Docetaxel (DTX) has been routinely used in the 1st and 2nd line treatment of various types of cancers, such as breast cancer, lung cancer, and prostate cancer (Imran et al. 2020). DTX exerts its cytotoxicity by promoting the assembly of tubulin into stable microtubules, while simultaneously preventing their disassembly (Ojima et al. 2016). However, its clinical application is primarily limited by poor water solubility and side effects (Ghassami et al. 2018). In some cases, multidrug resistance (MDR) can also be acquired due to various complex mechanisms, including the inhibition of the apoptosis pathway via the overexpression of NF-κB, activation of DNA repair, and enhanced drug efflux (Murray et al. 2012; Wang et al. 2015a, b). To overcome MDR, the use of synergistic drug combinations in place of single drug administration has been investigated to improve therapeutic outcomes (Qi et al. 2017; Liang et al. 2021).

The combination of curcumin (CUR) and DTX has been studied extensively (Batra et al. 2019). CUR can increase anti-proliferative activities through various pathways, for example, by inhibiting other transcription factors, such as cyclin D1, protein kinase B, and HIF-1α; interrupting the expression of p-glycoprotein; and downregulating the NF-κB pathway (Baek et al. 2017; Wei et al. 2017; Patel et al. 2020). Since CUR can enhance DTX activity by inhibiting the NF-κB signaling pathway and angiogenesis as a pro-apoptotic agent, CUR has been combined with DTX for increased efficacy in chemoresistant cancers (Batra et al. 2019). To achieve a synergistic anticancer activity, the combined DTX and CUR should be co-delivered to the same target at an optimal ratio (Zhang et al. 2016). However, this is challenging due to differences in the physical properties, rates of metabolism, and the pharmacokinetics and distribution of drugs within the body (Dai et al. 2017). In relation to the concept of combination therapy, much attention has been focused on the development of an alternative delivery system exploiting the nanotechnology that can maintain optimized synergistic drug ratios.

Various targeted nanocarrier systems using liposomes, nanoparticles, drug–polymer conjugates, and micelles have improved the effectiveness and decreased the side effects of cancer chemotherapy (Sun et al. 2021). Among the various nanocarrier systems, nanostructured lipid carriers (NLCs) show various advantageous properties, such as a high hydrophobic drug loading capacity, controlled release ability, and biocompatibility (Kim et al. 2017; Haider et al. 2020). Further, for prolonged circulation in vivo and target-specific delivery, the surface of NLCs can be functionalized with various targeting ligands or steric stabilizers, such as polyethylene glycol (PEG) (Rabanel et al. 2014; Bazak

et al. 2015). In this regard, our group had previously developed the IPLVVPLRRRRRR RRC (RIPL) peptide as a cell-penetrating and homing peptide and prepared PEGylated and RIPL peptide-conjugated NLCs (P/R-NLC) as a platform for hepsin-specific targeted drug delivery. P/R-NLCs can reach the tumor tissue via enhanced permeability and retention effect due to the prolonged circulation in vivo and can recognize and selectively bind to the hepsin on the cell membrane, subsequently being internalized via endocytosis (Kang et al. 2014; Rashidi et al. 2014; Shrestha et al. 2019). This significantly improved the anticancer effects of DTX in hepsin-overexpressing cancer (Kim et al. 2018, 2020). However, using this platform, no attempts have been made to attain synergistic effects during combination therapy.

In this study, we examined the co-administration of individual drug-loaded P/R-NLC systems to increase therapeutic efficacy in drug-resistant breast cancer cells. For this, DTX-loaded P/R-NLCs (DTX-P/R-NLC) and CUR-loaded P/R-NLCs (CUR-P/R-NLC) were prepared and their physicochemical characteristics, including storage stability and drug release kinetics, were evaluated. After optimizing the combination ratio, in vitro antitumor efficacy was assessed in terms of cytotoxicity, apoptosis, and cell cycle distribution. Finally, we assessed in vivo antitumor efficacy using an OVCAR3-xenografted mouse model.

## Results

### Characteristics of NLCs

Physicochemical characteristics, including nanoparticle size, polydispersity (PDI), zeta potential (ZP), drug loading (DL), and encapsulation efficiency (EE), of various NLCs were evaluated (Table 1). The compositions of the different NLC samples are summarized in Additional file 1: Table S1. The average size of the NLCs ranged from

**Table 1** Characteristics of docetaxel (DTX)- or curcumin (CUR)-loaded nanostructured lipid carriers (NLCs)

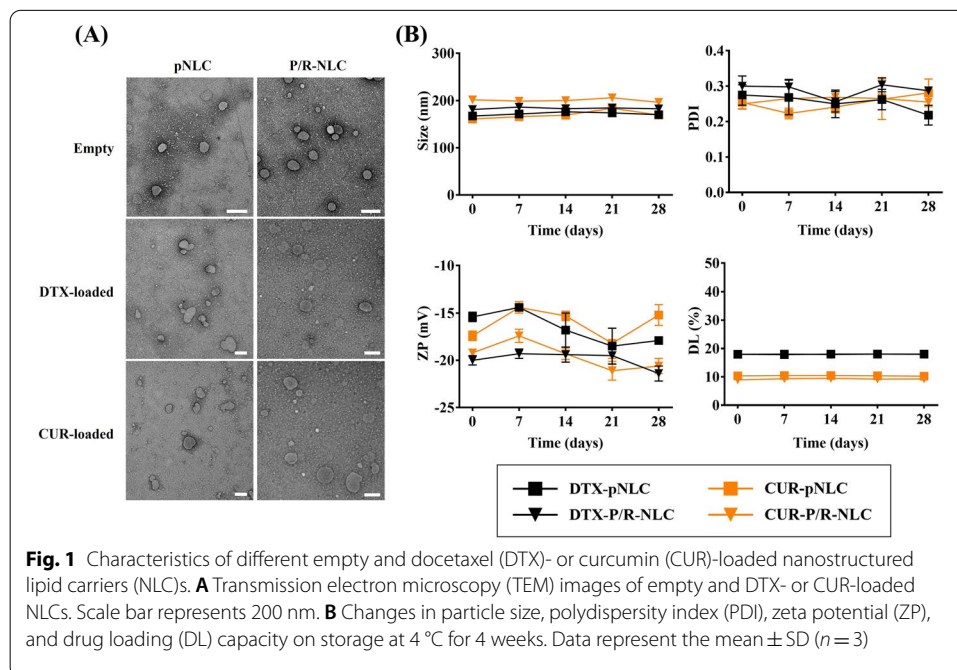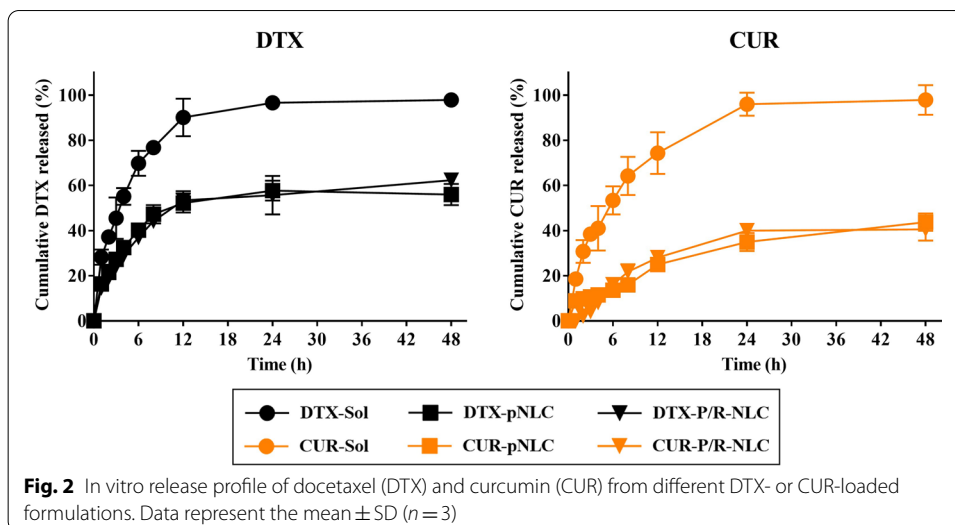|  | pNLCs | P/R-NLCs |
|---|---|---|
| *Empty* | | |
| Size (nm) | 161.4 ± 2.6 | 190.0 ± 4.8 |
| PDI | 0.277 ± 0.015 | 0.251 ± 0.011 |
| ZP (mV) | −18.5 ± 0.9 | −19.9 ± 0.8 |
| *DTX-loaded* | | |
| Size (nm) | 171.7 ± 6.4 | 192.4 ± 0.9 |
| PDI | 0.315 ± 0.024 | 0.249 ± 0.012 |
| ZP (mV) | −16.7 ± 0.2 | −17.2 ± 0.2 |
| EE (%) | 99.9 ± 0.01 | 99.2 ± 0.02 |
| DL (%) | 17.93 ± 0.04 | 17.96 ± 0.03 |
| *CUR-loaded* | | |
| Size (nm) | 161.0 ± 1.3 | 201.7 ± 1.2 |
| PDI | 0.254 ± 0.019 | 0.250 ± 0.014 |
| ZP (mV) | −17.4 ± 0.5 | −16.4 ± 0.3 |
| EE (%) | 99.9 ± 0.01 | 99.9 ± 0.01 |
| DL (%) | 10.31 ± 0.01 | 8.93 ± 0.01 |

Data represent the mean ± SD ($n = 3$)

DTX, docetaxel; CUR, curcumin; pNLCs, plain NLCs; P/R-NLCs, PEGylated and RIPL peptide-conjugated NLCs; PDI, polydispersity index; ZP, zeta potential; EE, encapsulation efficiency; DL, drug loading

approximately 160 to 200 nm, as determined by dynamic light scattering (DLS). As the size difference between empty NLCs and drug-encapsulated NLCs was not significant, drug encapsulation did not affect the size of the NLCs. Most PDI values were below 0.3, indicating a narrow and homogenous size distribution. In terms of ZP, all types of NLCs ranged from − 16 mV to − 20 mV. DL was observed as approximately 18% for DTX-loaded NLCs and 8.9–10.3% for CUR-loaded NLCs. Regardless of the drugs or formulation type, EE (%) represented a high value of almost 99%. Transmission electron microscopy (TEM) images showed various types of NLCs that were spheroid, with an average size of approximately 200 nm, exhibiting no particle aggregation, and having high colloidal stability (Fig. 1A).

### Stability of NLC formulations

The storage stability of DTX- or CUR-loaded NLCs was evaluated at $4 \pm 1$ °C for 28 days by analyzing the particle size, PDI, ZP, and DL (Fig. 1B). During this period, no changes were observed in the appearance of the NLC formulations. Regardless of the encapsulated drug type, the particle size and PDI remained around 200 nm and below 0.3, respectively. Further, the absolute value of ZP was maintained above 15 mV and there were no significant differences compared to the values from the initial day. Further, NLC formulations maintained the high DL for 28 days. There was no change in EE compared to the initial value; in other words, the stability of the NLC samples was well-maintained without leakage under storage conditions. Also, in the serum containing RPMI 1640 cell culture media, the NLC formulations remained stable without significant changes in size, ZP, and PDI or drug leakage (Additional file 1: Fig. S1). Consequently, all prepared NLCs maintained their colloidal stability under the storage conditions for 4 weeks



**Fig. 1** Characteristics of different empty and docetaxel (DTX)- or curcumin (CUR)-loaded nanostructured lipid carriers (NLC)s. **A** Transmission electron microscopy (TEM) images of empty and DTX- or CUR-loaded NLCs. Scale bar represents 200 nm. **B** Changes in particle size, polydispersity index (PDI), zeta potential (ZP), and drug loading (DL) capacity on storage at 4 °C for 4 weeks. Data represent the mean $\pm$ SD ($n = 3$)

Kim *et al. Cancer Nanotechnology* (2022) 13:17

Page 5 of 26



**Fig. 2** In vitro release profile of docetaxel (DTX) and curcumin (CUR) from different DTX- or CUR-loaded formulations. Data represent the mean ± SD ($n = 3$)

**Table 2** Kinetic modeling of docetaxel (DTX) and curcumin (CUR) release from different nanoparticle formulations

|  | Zero-order | | First-order | | Higuchi | |
|---|---|---|---|---|---|---|
|  | $K_0$ (µg/h) | $r^2$ | $K_1$ ($h^{-1}$) | $r^2$ | $K_H$ ($h^{-0.5}$) | $r^2$ |
| DTX-pNLC | 2.0776 | 0.7027 | 0.0145 | 0.7957 | 15.7216 | 0.9920 |
| DTX-P/R-NLC | 2.1034 | 0.7254 | 0.0143 | 0.7976 | 15.6762 | 0.9954 |
| CUR-pNLC | 0.8423 | 0.8873 | 0.0050 | 0.9287 | 6.5096 | 0.9765 |
| CUR-P/R-NLC | 1.7106 | 0.9057 | 0.0097 | 0.9435 | 9.1374 | 0.9476 |

$K_0$, zero-order rate constant; $K_1$, first-order rate constant; $K_H$, Higuchi equation's rate constant; $r^2$, correlation coefficient

pNLC, plain nanostructured lipid carrier; P/R-NLC, PEGylated and RIPL peptide-conjugated nanostructured lipid carrier

and physiological condition for 48 h without signs of aggregation until their use in the experiments.

### In vitro drug release profile

Results of the in vitro release assay for DTX or CUR (48 h) are shown in Fig. 2. Results of the in vitro release assay for DTX or CUR (48 h) are shown in Fig. 2. The drug release from both DTX-containing solution (DTX-Sol) and CUR-containing solution (CUR-Sol) reached almost 50% at 6 h and increased to 90% and 70% at 12 h, respectively. Particularly in the early period, drug release from both solution samples was exceptionally retarded, possibly due to the micelle formation in DTX-Sol and/or drug precipitation in CUR-Sol by serial dilution. In contrast, DTX- or CUR-loaded NLC formulations showed a slow and sustained release pattern. DTX release from DTX-loaded plain NLCs (DTX-pNLCs) and DTX-P/R-NLCs measured about 52% and 53% at 12 h, respectively, followed by a release rate plateau for both after 24 h. In contrast, CUR release from CUR-loaded plain NLCs (CUR-pNLCs) and CUR-P/R-NLCs measured 25% and 28% at 12 h, respectively, and slowly increased to approximately 40% at 24 h. Data obtained from the mathematical equations are listed in Table 2. The release of the DTX-pNLCs,

Kim *et al. Cancer Nanotechnology*     (2022) 13:17
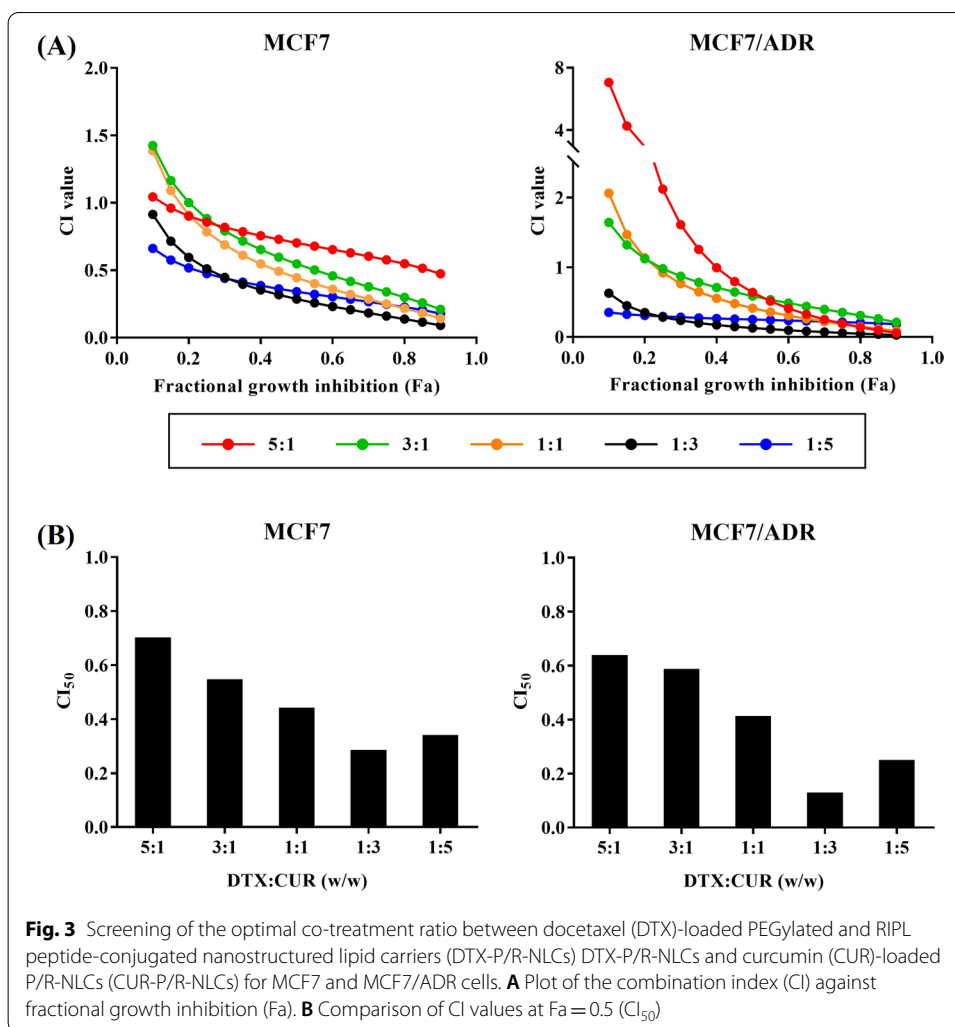
Page 6 of 26

CUR-pNLCs, DTX-P/R-NLCs, and CUR-P/R-NLCs was best fitted in the Higuchi equation with $r^2$ values of 0.9920, 0.9954, 0.9765, and 0.9476, respectively, suggesting a diffusion-controlled drug release. The release rate constants of DTX-loaded NLC samples were greater than those of CUR-loaded NLC samples, which might be due to the relatively higher drug loading of DTX compared to CUR. Formulation difference between pNLC and P/R-NLC was negligible for DTX-loaded samples, although the difference was somewhat increased for CUR-loaded samples.

**In vitro screening of DTX-P/R-NLCs and CUR-P/R-NLCs**

To determine the synergistic ratio of DTX and CUR, the 3-(4,5-dimethyl-2-thiazolyl)-2,5-diphenyl-2H-tetrazolium bromide (MTT) assay was used to evaluate the cell viability of MCF7 and MCF7/ADR cells after incubation with DTX-P/R-NLCs and CUR-P/R-NLCs either alone or in combination with different weight ratios (DTX:CUR = 5:1, 3:1, 1:1, 1:3, and 1:5, w/w) for 24 h. The cytotoxicity of the drug combinations was evaluated by measuring the quantity of formazan that is proportionally produced to the number of viable cells. The untreated cells were taken as control with 100% viability. The cytotoxicity of the different combination ratios of DTX-P/R-NLCs and CUR-P/R-NLCs showed a concentration-dependent trend (Additional file 1: Fig. S2). The median effect analysis, described by Chou and Talaly, and combination index (CI) were used to determine the synergistic inhibitory effect (CI < 1, synergy; CI = 1, additivity; and CI > 1, antagonism). As shown in Fig. 3A, the combination of DTX-P/R-NLCs and CUR-P/R-NLCs showed synergistic effects in both cell lines. All combination ratios at 0.5 fractional growth inhibition (Fa; Fa = 0 represents 100% cell viability; Fa = 1 represents 0% cell viability) revealed a CI value of < 1, signifying a synergistic mechanism of action (Fig. 3B). Moreover, the lowest CI value was observed at a weight ratio of 1:3 (DTX:CUR) in both cell lines. Since a strong synergism was observed at a ratio of 1:3, with a CI value of 0.285 and 0.129 in MCF7 and MCF7/ADR cells, respectively, the DTX:CUR ratio of 1:3 was selected as the optimal combination ratio for the subsequent experiments.

**Cytotoxicity evaluation**

Next, we employed the MTT assay to determine the in vitro cytotoxicity of various DTX- or CUR-loaded formulations and the formulations containing either DTX or CUR against MCF7 and MCF7/ADR cells at different concentrations in 24 h. Cell viability in the untreated group was considered as 100%. Based on the CI, the weight ratio of DTX and CUR for co-treatment was fixed at 1:3 (DTX:CUR). All empty formulations revealed no significant cell death in the concentration range used in this experiment (Fig. S3), whereas DTX- or CUR-loaded formulations or the co-treatment formulations showed dose-dependent cytotoxicity in both cell lines (Fig. 4). In both cell lines, the cytotoxicity of DTX increased when administered in combination with CUR due to the synergistic cytotoxic effect of CUR. For further comparison, half-maximal inhibitory concentration ($IC_{50}$) values for different drug-loaded formulations were calculated. As summarized in Table 3, $IC_{50}$ values decreased depending on the formulations regardless of the drug in the following order in both cell lines: free drug > pNLCs > P/R-NLCs. MCF7/ADR cells (drug-resistant) required a higher dose of DTX or CUR to achieve the same level of cell death as MCF7 cells (drug-sensitive). The co-treatment of DTX and CUR demonstrated

**Fig. 3** Screening of the optimal co-treatment ratio between docetaxel (DTX)-loaded PEGylated and RIPL peptide-conjugated nanostructured lipid carriers (DTX-P/R-NLCs) DTX-P/R-NLCs and curcumin (CUR)-loaded P/R-NLCs (CUR-P/R-NLCs) for MCF7 and MCF7/ADR cells. **A** Plot of the combination index (CI) against fractional growth inhibition (Fa). **B** Comparison of CI values at Fa = 0.5 (CI$_{50}$)

an improved performance compared to the single-drug treatment (free drug solution or P/R-NLCs) over a range of concentrations, with a lower IC$_{50}$ value and small CI value under 1. In both MCF7 and MCF7/ADR cells, the combination of DTX-P/R-NLC and CUR-P/R-NLC exhibited greater synergism compared to the combination of DTX-Sol and CUR-Sol.

### Cell apoptosis analysis

Cell apoptosis was evaluated quantitatively to confirm the enhanced apoptotic ability of DTX- or CUR-loaded formulations using the fluorescein isothiocyanate (FITC)-annexin V/propidium iodide (PI) staining assay. In Fig. 5A, the flow cytometric quadrantal diagram is divided into four parts to interpret apoptotic tendency. The lower left (Q1), lower right (Q2), upper left (Q3), and upper right (Q4) quadrants indicate viable, early apoptotic, late apoptotic, and necrotic regions, respectively. In both cell lines, very low level of apoptosis was detected in the untreated controls and CUR-only formulations, whereas the DTX formulations significantly increased total apoptosis rates. Figure 5B represents the percentage of early and late apoptotic MCF7 and MCF7/ADR cells treated

Kim *et al. Cancer Nanotechnology*     (2022) 13:17

Page 8 of 26
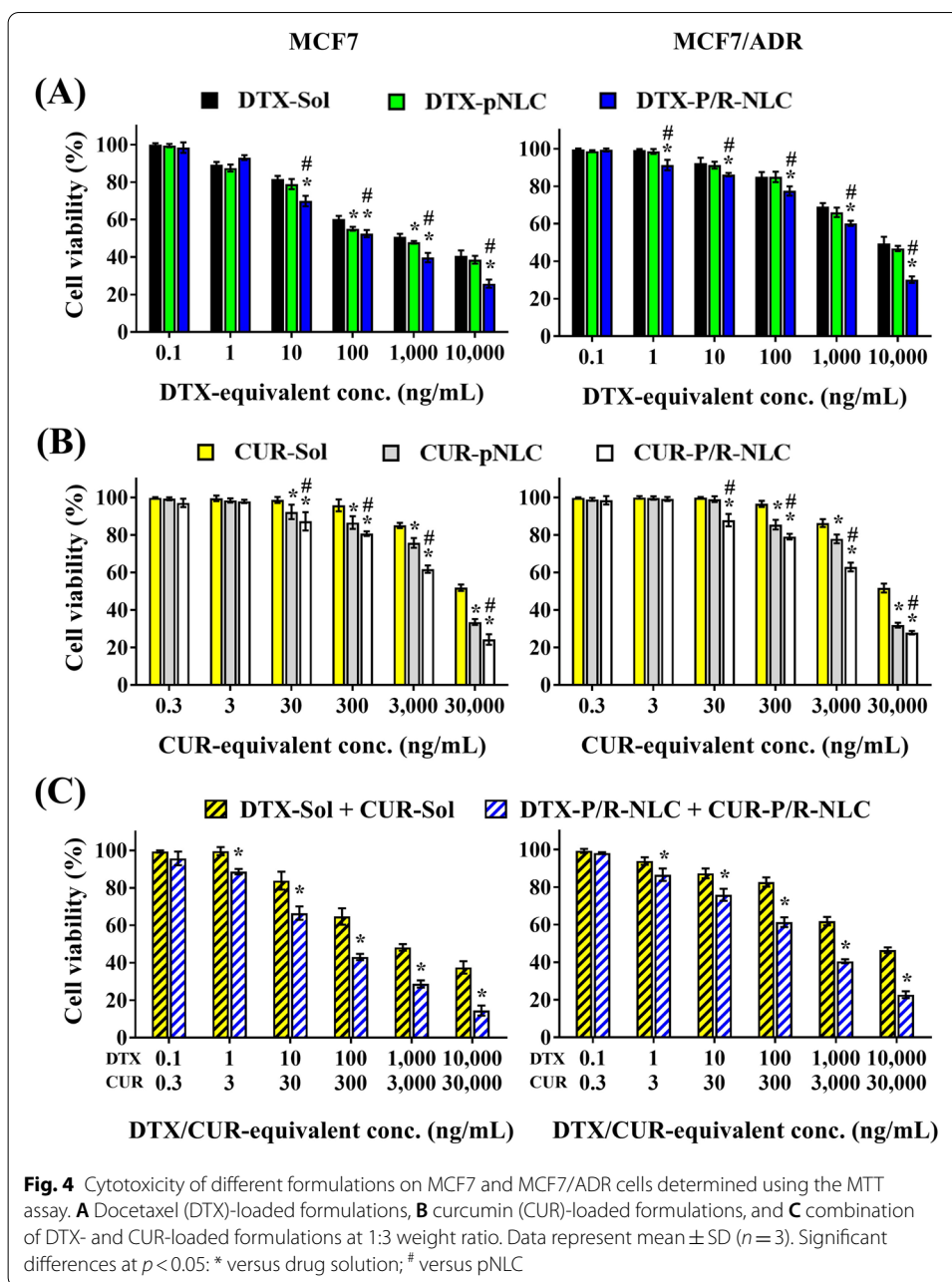


**Fig. 4** Cytotoxicity of different formulations on MCF7 and MCF7/ADR cells determined using the MTT assay. **A** Docetaxel (DTX)-loaded formulations, **B** curcumin (CUR)-loaded formulations, and **C** combination of DTX- and CUR-loaded formulations at 1:3 weight ratio. Data represent mean ± SD ($n = 3$). Significant differences at $p < 0.05$: * versus drug solution; # versus pNLC

with various combinations of DTX- and CUR-loaded formulations. DTX-Sol, DTX-pNLCs, and DTX-P/R-NLCs induced 15.9 ± 1.0%, 17.2 ± 0.3%, and 19.3 ± 1.2% MCF7 cell apoptosis and 11.9 ± 0.7%, 14.1 ± 1.1%, and 16.5 ± 0.9% MCF7/ADR cell apoptosis, respectively. The combination of DTX and CUR significantly increased the apoptotic effect in both MCF7 and MCF7/ADR cells. Compared to DTX-Sol single treatment, the combination of DTX-Sol and CUR-Sol and the combination of DTX-P/R-NLCs and CUR-P/R-NLCs exhibited a 1.5- and 1.3-fold increase in the apoptosis rate of MCF7 and MCF7/ADR cells, respectively.

Kim *et al. Cancer Nanotechnology* (2022) 13:17

Page 9 of 26

**Table 3** Half-maximal inhibitory concentration ($IC_{50}$) and combination index (CI) values for different docetaxel (DTX)- or curcumin (CUR)-loaded formulations against MCF7 and MCF7/ADR cell lines

| Sample | $IC_{50}$ (ng/mL) | | CI (Fa = 0.5) |
|---|---|---|---|
| | DTX-equivalent | CUR-equivalent | |
| *MCF7* | | | |
| DTX-Sol | 1,000.5 ± 68.5 | n/a | n/a |
| DTX-pNLC | 650.3 ± 79.5 | n/a | n/a |
| DTX-P/R-NLC | 134.1 ± 8.1 | n/a | n/a |
| CUR-Sol | n/a | 29,884.5 ± 2,336.6 | n/a |
| CUR-pNLC | n/a | 12,008.5 ± 1,071.8 | n/a |
| CUR-P/R-NLC | n/a | 5,361.0 ± 386.8 | n/a |
| DTX-Sol + CUR-Sol | 876.9 ± 204.8 | 2,631.0 ± 614.8 | 0.964 |
| DTX-P/R-NLC + CUR-P/R-NLC | 59.8 ± 12.3 | 179.4 ± 37.0 | 0.479 |
| *MCF7/ADR* | | | |
| DTX-Sol | 6,166.8 ± 325.7 | n/a | n/a |
| DTX-pNLC | 5,422.3 ± 564.6 | n/a | n/a |
| DTX-P/R-NLC | 1,704.8 ± 141.4 | n/a | n/a |
| CUR-Sol | n/a | 29,954.3 ± 3,781.2 | n/a |
| CUR-pNLC | n/a | 11,840.5 ± 206.6 | n/a |
| CUR-P/R-NLC | n/a | 5,569.8 ± 344.1 | n/a |
| DTX-Sol + CUR-Sol | 3,325.3 ± 778.1 | 9,976 ± 2,333.6 | 0.822 |
| DTX-P/R-NLC + CUR-P/R-NLC | 347.6 ± 73.3 | 1,042.8 ± 220.1 | 0.389 |

Data represent the mean ± SD ($n = 3$)

DTX-Sol, DTX-containing solution; CUR-Sol, CUR-containing solution; pNLC, plain nanostructured lipid carrier; P/R-NLC, PEGylated and RIPL peptide-conjugated nanostructured lipid carrier; $IC_{50}$, half-maximal inhibitory concentration; CI, combination index; Fa, fractional growth inhibition; n/a, not available

## Cell cycle analysis

'The effects of free drugs and drug-loaded NLC samples on cell cycle progression in MCF7 and MCF7/ADR cells were measured by analyzing the cellular DNA content using flow cytometry. By measuring the fluorescence of the stained nucleus, the percentage of cell population in each phase of the cell cycle could be determined based on the DNA present. The number of cells was plotted against the relative fluorescence intensity of PI (FL2 channel). As shown in Fig. 6, compared to the untreated group, the cell population of the section divided by the gate changed in the drug-treated groups. Most of the untreated MCF7 and MCF7/ADR cells were in the G0/G1 phase, and approximately 18.74% and 21.53% of the MCF7 and MCF7/ADR cells were distributed in the G2/M phase, respectively. In both cell lines, the treatment with CUR-loaded formulations or empty-P/R-NLCs showed that cells were primarily distributed in the G0/G1 phase without any increase in the proportion of cells in the subG0 or G2/M phases. In contrast, all DTX treatments significantly reduced the percentage of cells in the G0/G1 phase and increased that of the cells in the G2/M or subG0 phases. As seen in the bar graphs in Fig. 6A, the population of MCF7 cells in the G2/M phase increased to 35.82, 35.11, and 36.41% after incubation with DTX-Sol, DTX-pNLCs, and DTX-P/R-NLCs, respectively. A similar cell cycle distribution was observed in MCF7 cells following the combination treatment with DTX and CUR. Compared with the control cells, treatment of the MCF7/ADR cells with DTX formulations resulted in the arrest of the cells in the subG0 phase (Fig. 6B). The percentage of MCF7/ADR cells treated with DTX-Sol,
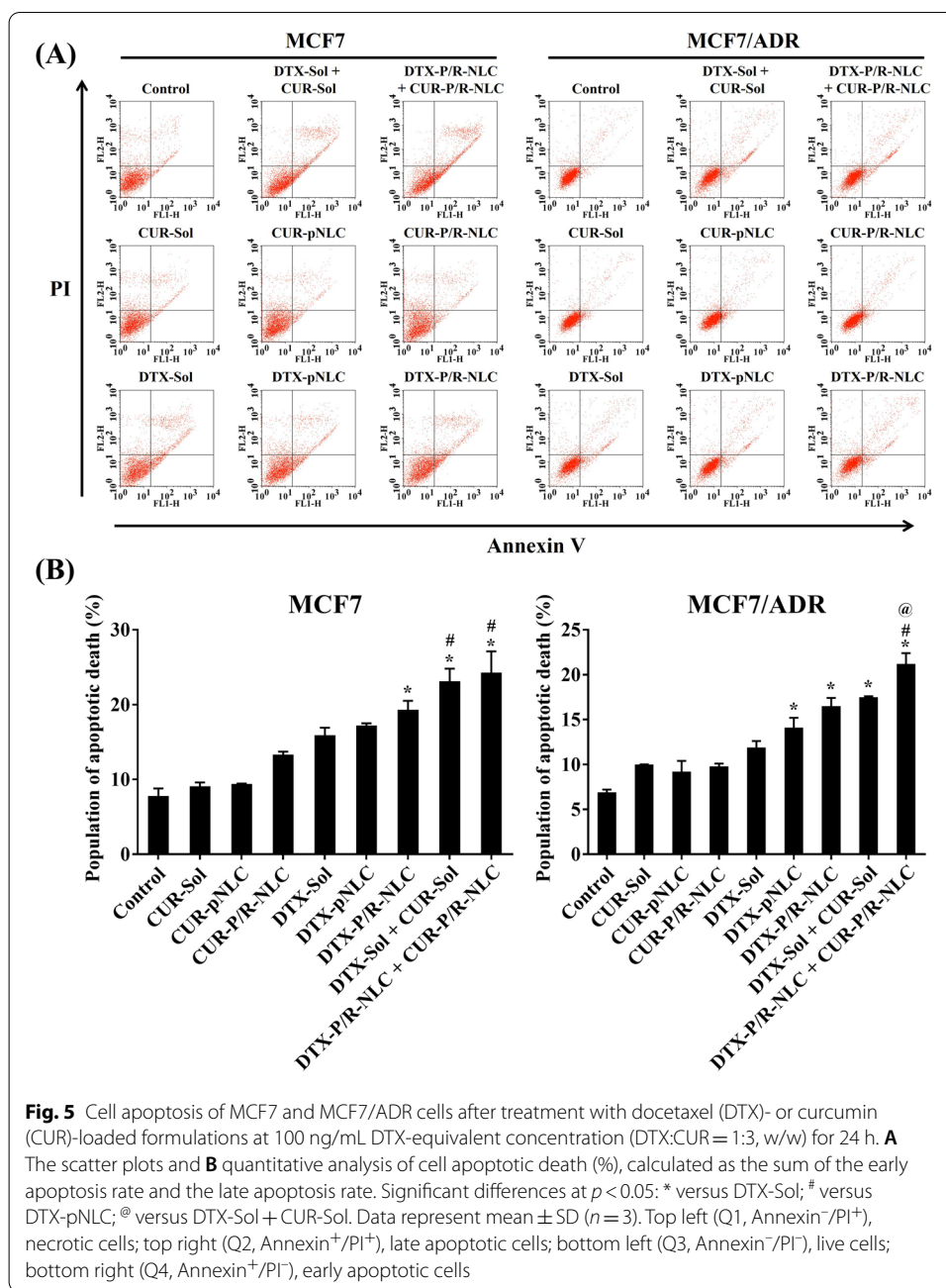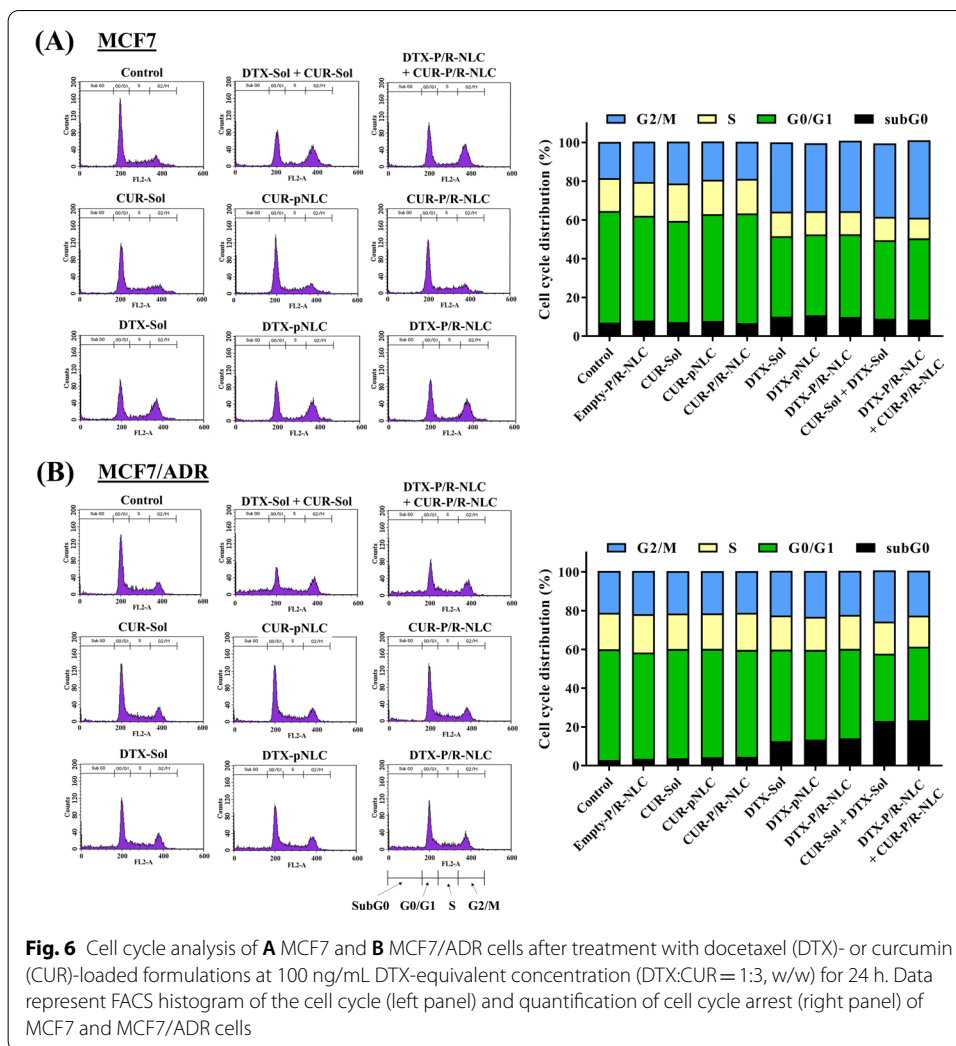
**Fig. 5** Cell apoptosis of MCF7 and MCF7/ADR cells after treatment with docetaxel (DTX)- or curcumin (CUR)-loaded formulations at 100 ng/mL DTX-equivalent concentration (DTX:CUR = 1:3, w/w) for 24 h. **A** The scatter plots and **B** quantitative analysis of cell apoptotic death (%), calculated as the sum of the early apoptosis rate and the late apoptosis rate. Significant differences at $p < 0.05$: * versus DTX-Sol; # versus DTX-pNLC; @ versus DTX-Sol + CUR-Sol. Data represent mean ± SD ($n = 3$). Top left (Q1, Annexin$^-$/PI$^+$), necrotic cells; top right (Q2, Annexin$^+$/PI$^+$), late apoptotic cells; bottom left (Q3, Annexin$^-$/PI$^-$), live cells; bottom right (Q4, Annexin$^+$/PI$^-$), early apoptotic cells
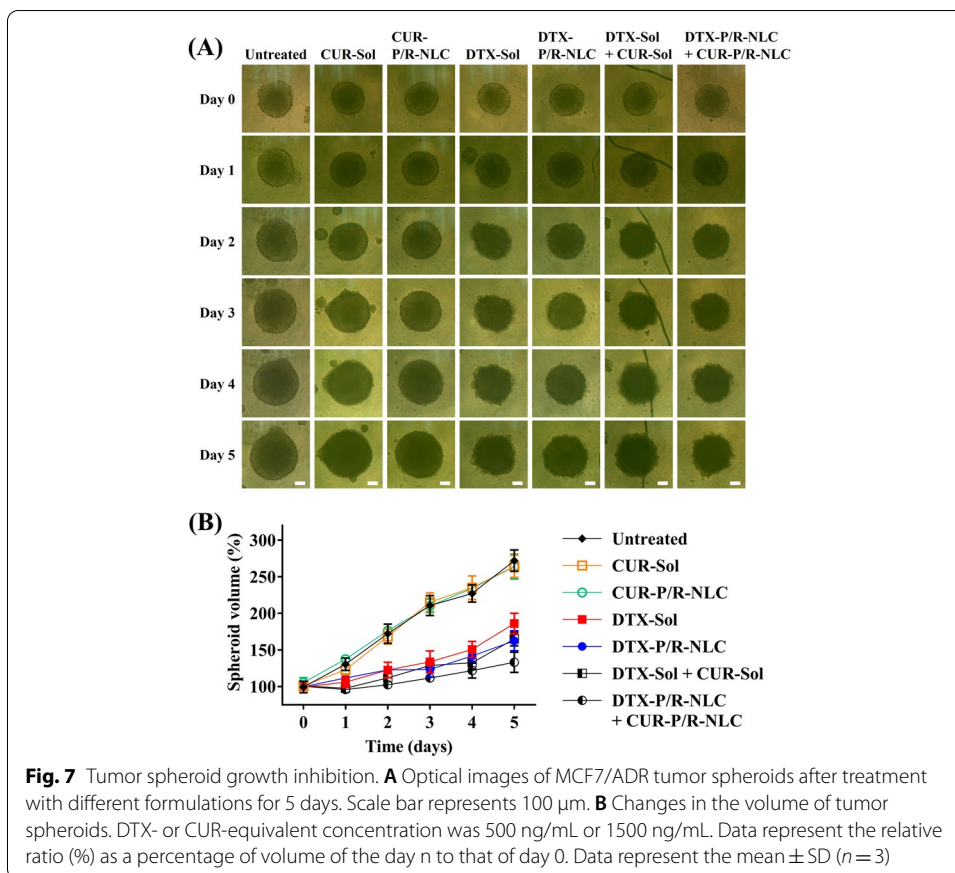
DTX-pNLCs, and DTX-P/R-NLCs in the subG0 phase increased to 12.72%, 13.41%, and 14.11%, respectively. Importantly, the combination treatment of DTX-Sol and CUR-Sol and that of DTX-P/R-NLCs and CUR-P/R-NLCs induced significantly higher subG0 arrest of the cell populations (23.04% and 23.42%, respectively) compared to the DTX-only treatment.

### Tumor spheroid growth inhibition

The growth inhibition of MCF7/ADR tumor spheroids was evaluated after treatment with different DTX- or CUR-loaded formulations. The tumor spheroids were
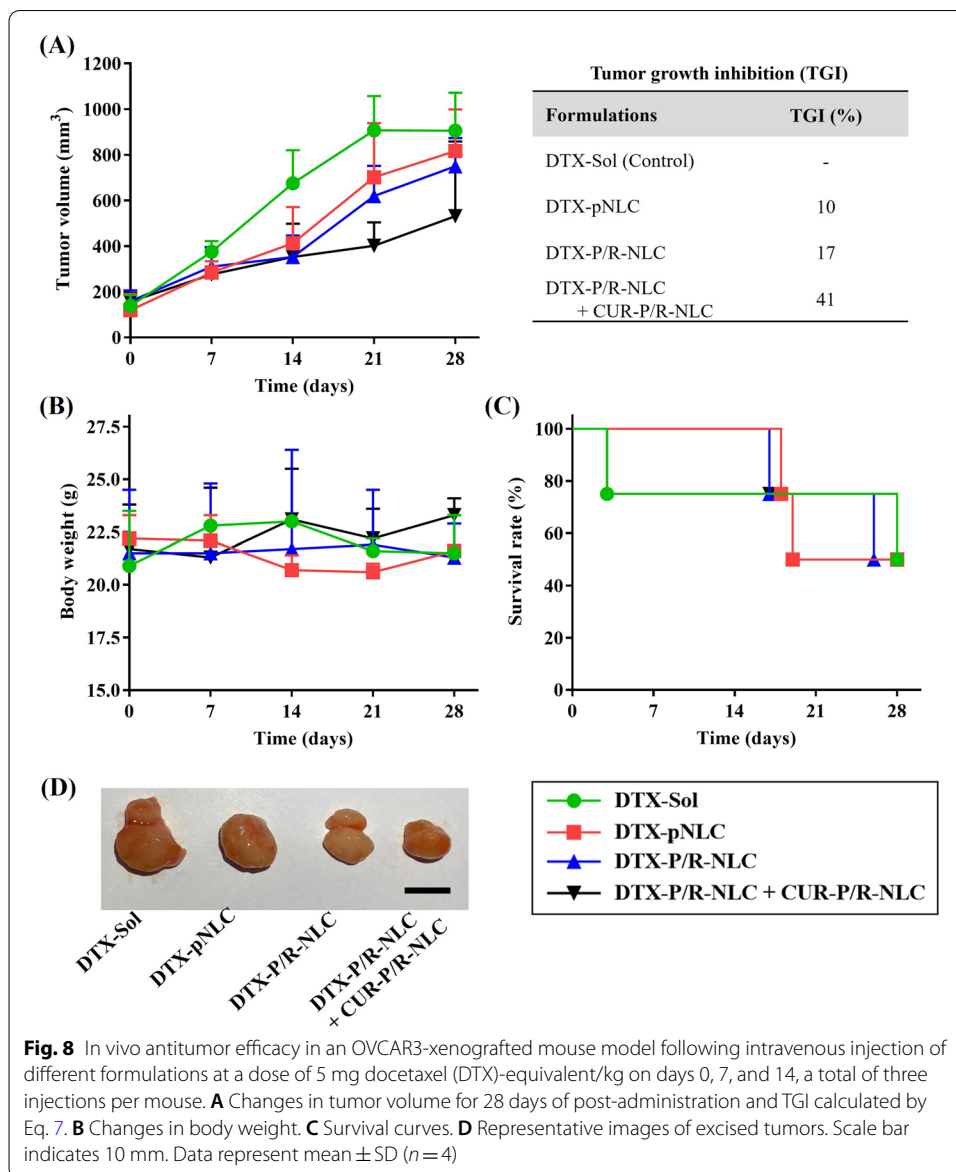
**Fig. 6** Cell cycle analysis of **A** MCF7 and **B** MCF7/ADR cells after treatment with docetaxel (DTX)- or curcumin (CUR)-loaded formulations at 100 ng/mL DTX-equivalent concentration (DTX:CUR = 1:3, w/w) for 24 h. Data represent FACS histogram of the cell cycle (left panel) and quantification of cell cycle arrest (right panel) of MCF7 and MCF7/ADR cells

monitored for 5 days and brightfield images were captured every day to measure their diameter and assess morphological changes. As shown in Fig. 7A, the MCF7/ADR tumor spheroids were formed with a diameter of 350 μm and their size gradually increased until day 5, while maintaining their spherical shape. In Fig. 7B, the volume change ratio of the tumor spheroids was also calculated as a volume percentage from day n to day 0. MCF7/ADR tumor spheroids treated with CUR-Sol and CUR-P/R-NLCs showed no growth inhibition, evidencing the lack of cytotoxicity at the tested concentration of CUR, regardless of the formulation. Tumor spheroid volumes at day 5 in the untreated control, and CUR-Sol- and CUR-P/R-NLC-treated groups increased drastically up to 272%, 264%, and 263%, respectively. In contrast, DTX-containing groups displayed significantly higher and time-dependent inhibitory effects on the growth of MCF7/ADR tumor spheroids from day 2 to day 5. The volumes of MCF7/ADR tumor spheroids treated with DTX-Sol and DTX-P/R-NLCs increased to 186% and 162%, respectively. The co-treatment of DTX and CUR showed even greater tumor spheroid growth inhibition effects compared to the single-drug formulations. The combination of DTX-Sol and CUR-Sol and the

**Fig. 7** Tumor spheroid growth inhibition. **A** Optical images of MCF7/ADR tumor spheroids after treatment with different formulations for 5 days. Scale bar represents 100 μm. **B** Changes in the volume of tumor spheroids. DTX- or CUR-equivalent concentration was 500 ng/mL or 1500 ng/mL. Data represent the relative ratio (%) as a percentage of volume of the day n to that of day 0. Data represent the mean $\pm$ SD ($n = 3$)

combination of DTX-P/R-NLCs and CUR-P/R-NLCs exhibited the greatest inhibition of tumor spheroid growth (133%).

### In vivo antitumor efficacy

In vivo antitumor efficacy was evaluated in a BALB/c OVCAR3-bearing xenograft mouse model, in which the tumor developed over approximately 4 weeks following the subcutaneous inoculation of the OVCAR3 cell lines. As shown in Fig. 8A, the tumor grew exponentially in all groups. Compared to the DTX-Sol group, DTX-loaded NLC formulations were effective in reducing the tumor growth after 2 weeks of treatment. In comparison to the mild tumor-suppressive effect of DTX-pNLCs and DTX-P/R-NLCs, the combination group showed considerable inhibition of tumor growth after 3 weeks. At the end of the experiment (day 28), tumor volumes reached approximately 905, 816, 750, and 531 mm$^3$ in DTX-Sol, DTX-pNLC, DTX-P/R-NLC, and the combination of DTX-P/R-NLC and CUR-P/R-NLC groups, respectively. In particular, the combination group exhibited favorable tumor suppression, showing 1.7- and 1.4-fold greater inhibition compared with the DTX-Sol and DTX-P/R-NLC groups, respectively. The relative tumor volumes were expressed as tumor growth inhibition (TGI) percentages (insert table in Fig. 8A). The combination group produced a TGI value of 41%, which was higher than that of DTX-P/R-NLC (17%) and DTX-pNLC (10%). As depicted in Fig. 8B, the body weight changes of tumor-bearing mice were also recorded as an indication of safety. There was no significant difference

**Fig. 8** In vivo antitumor efficacy in an OVCAR3-xenografted mouse model following intravenous injection of different formulations at a dose of 5 mg docetaxel (DTX)-equivalent/kg on days 0, 7, and 14, a total of three injections per mouse. **A** Changes in tumor volume for 28 days of post-administration and TGI calculated by Eq. 7. **B** Changes in body weight. **C** Survival curves. **D** Representative images of excised tumors. Scale bar indicates 10 mm. Data represent mean $\pm$ SD ($n = 4$)

between the treatment groups. However, as the tumor volumes increased, the mice treated with DTX-Sol exhibited behavioral changes, such as impaired movement, loss of activity, and dry skin, whereas no obvious change was observed in the groups treated with DTX-pNLCs and DTX-P/R-NLCs and in the combination treatment group. Figure 8C depicts the survival curves, where the first death was observed in the DTX-Sol group on day 3, followed by the DTX-P/R-NLC, the combination of DTX-P/R-NLC and CUR-P/R-NLC, and the DTX-pNLC groups on days 17, 17, and 18, respectively. At the end of the experiment, 50% of the mice survived in all groups, and the excised tumors were photographed for further comparison (Fig. 8D). Tumor growth was greatly suppressed by the combination of DTX-P/R-NLCs and CUR-P/R-NLCs.

## Discussion

The co-delivery of two or more drugs to the disease site, using a nano-particulate carrier system, to achieve a synergistic effect is expected to emerge as a more efficient strategy than the current drug cocktail therapy (Zhang et al. 2016; Liang et al. 2021). Combination therapy using nanocarriers can maximize the therapeutic outcomes by resolving the issue of the poor water solubility of various drugs, by controlling the drug–drug ratio at the target site, and by increasing bioavailability owing to prolonged circulation and target-specific accumulation (Dai et al. 2017; Qi et al. 2017). Nanocarrier-mediated combination therapy can be distinguished based on the delivery mechanism of the drugs: (1) co-administration of different single drug-loaded nanocarriers, and (2) co-delivery of two or more therapeutic agents in a single nanocarrier system (Zhang et al. 2016; Dai et al. 2017). Compared to a single carrier system, the use of two separate nanocarriers to load each drug offers several advantages, such as avoiding the drug–drug interaction and its effects on individual drug efficacy, lowered drug toxicity, greater stability and loading capacity. Further, it is easy to control the quality of single-drug nanocarriers and to scale-up their preparation (Dai et al. 2017). Therefore, to construct a co-administrative nanoplatform for DTX and CUR, we used the previously reported P/R-NLC system developed for hepsin-specific active targeting with reduced mononuclear phagocyte uptake in vivo (Kim et al. 2018, 2020). Herein, DTX and CUR were encapsulated separately in P/R-NLCs, and each P/R-NLC (DTX-P/R-NLC and CUR-P/R-NLC) was physically mixed for the combined application.

In the present study, two types of DTX- or CUR-loaded NLCs (pNLCs and P/R-NLCs) were successfully prepared using the solvent emulsification–evaporation method. The encapsulation of DTX or CUR did not alter the size of the NLCs, but surface-modification with PEG3K and RIPL peptide slightly increased the size to approximately 200 nm. Due to their nano-size of less than 200 nm, P/R-NLCs can accumulate in tumor tissues by virtue of the enhanced permeability and retention effect and readily translocate into cancer cells via receptor-mediated endocytosis (Kebebe et al. 2018; Kondo et al. 2021). ZP is a key parameter in the evaluation of the stability of nanocarriers. The repulsion of the nanocarriers with same surface charge provides extra colloidal stability (Ribeiro et al. 2016). All prepared NLCs, regardless of the type of encapsulated drug, exhibited negative charge with an absolute ZP value above 15 mV, indicating sufficient electrostatic repulsion. This result was in accordance with an earlier report that PEG and RIPL peptide modification imparted negative charge on the surface of NLCs (Kim et al. 2018). Consequently, all obtained NLCs maintained their colloidal stability under storage conditions for 4 weeks without signs of aggregation or changes in DL.

The synergistic mass ratio of DTX and CUR for combination therapy was selected after calculating the CI in MCF7 and MCF7/ADR cells. Interestingly, for the combination of DTX-P/R-NLCs and CUR-P/R-NLCs, we found that the mass ratio of 1:3 resulted in the strongest synergistic effects among four tested mass ratios. The specific cellular uptake of P/R-NLCs and DTX or CUR released from the NLC matrix may influence the drug–drug ratio in the cytosol. The free drugs enter the cells through diffusion, which is related to the physicochemical properties of the drugs (Shi et al. 2015). Presence of free DTX and CUR may lead to different uptake behaviors, and accordingly, the mass ratio of the drugs inside the cells may be become inconsistent

with the initial mass ratio. The co-administered DTX-P/R-NLCs and CUR-P/R-NLCs bind to the overexpressed hepsin on tumor cell membranes (Kim et al. 2020). DTX-P/R-NLCs and CUR-P/R-NLCs are internalized via receptor-mediated endocytosis, in which the two nanocarrier systems are internalized as a whole, which helps maintain the loading mass ratio (Xu et al. 2019). Upon internalization, both DTX and CUR are released from the NLCs, and the intracellular ratio of the drugs may vary depending on the release pattern. DTX- or CUR-loaded P/R-NLCs followed the Higuchi equation, indicating homogenous drug dispersion through the lipid matrix and diffusion-controlled release by matrix erosion and degradation (Son et al. 2017). Due to the higher drug loading of DTX, it may show a relatively faster release than CUR. Based on the findings our drug loading and release experiments, the mass ratio of 1:3 (DTX:CUR, w/w) for DTX-P/R-NLCs and CUR-P/R-NLCs was selected as the optimal combination ratio and was applied for further experiments.

Cytotoxicity of DTX- or CUR-loaded formulations in MCF7 and MCF7/ADR cells was evaluated using the MTT assay. Treatment with DTX- or CUR-loaded formulations showed time- and concentration-dependent effects on cell viability. The $IC_{50}$ values at 24 h were in the order of P/R-NLCs < pNLCs < free drugs, indicating the importance of RIPL peptide exposure on the surface of NLCs. Co-treatment with DTX and CUR exhibited a better performance than treatment with the individual drugs. The antitumor effect of DTX- or CUR-loaded formulations was also evaluated in MCF7/ADR 3D spheroids by measuring the tumor growth inhibition. The changes in the volumes of 3D tumor spheroids were consistent with the trend of $IC_{50}$ in cell viability experiments. The lower the $IC_{50}$ value, the greater the inhibition effect on the volume of 3D tumor spheroids. The cytotoxicity of CUR-only treatments was low with negligible effect, because the concentration of CUR was insufficient to affect cell viability. In contrast, the combination of DTX and CUR showed the greater tumor spheroid inhibition compared with the DTX-only treatments. Our data supported the earlier reports that CUR enhanced the antitumor efficacy of DTX by acting as a pro-apoptotic agent via well-known signaling pathway (Misra et al. 2011; Yang et al. 2017a, b).

The anticancer effect of DTX- or CUR-loaded formulations was further confirmed using the FITC-annexin V/PI-based apoptosis assay. The effects of DTX- or CUR-loaded formulations on the apoptosis of MCF7 and MCF7/ADR cells were consistent with the results of the cytotoxicity assay. As shown in Fig. 5B, in comparison to the untreated control, the induction of cell apoptosis by treating with CUR-only formulations was insignificant, whereas it was significantly increased by the combination with DTX. The data clearly reveal that treatment with a combination of DTX-P/R-NLCs and CUR-P/R-NLCs led to an increase in apoptotic cell death compared to the treatment with single DTX-loaded formulations. Since all empty formulations caused no significant cell death with good tolerability and low toxicity, the differences in the cytotoxic and apoptotic effects of DTX- or CUR-loaded NLC formulations are attributed to the drug concentrations in the cytoplasm. For free drug solutions, internalization occurs mainly by molecular diffusion and the drug concentration increases until saturation (Shi et al. 2015). However, NLCs mainly intracellularly translocate via endocytosis and release the encapsulated drug into the cytoplasm in a controlled

manner. In a previous study, we found that P/R-NLCs induced RIPL-mediated internalization via endocytosis into hepsin-overexpressing cancer cells, showing strong cytosolic fluorescence intensity without premature fluorescent probe release (Kim et al. 2018). Taken together, these observations demonstrate that the superior in vitro antitumor effects of the combined administration of DTX-P/R-NLCs and CUR-P/R-NLCs are due to the enhanced intracellular uptake of DTX and CUR and the subsequent intracellular release that both facilitate high intracellular concentrations of DTX and CUR for synergy.

To collect more evidence regarding the apoptotic activity of DTX and the cell death pathway activity, the cell cycle distribution for MCF7 and MCF7/ADR cells was analyzed using flow cytometry. It is well-known that DTX exerts its antitumor effect by binding to β-tubulin, thereby inducing microtubule stabilization resulting in G2/M arrest and the subsequent apoptotic cell death (Murray et al. 2012; Ojima et al. 2016). In MCF7 cells, DTX-containing treatments enhanced the accumulation of the cells in the G2/M phase after a 24 h incubation (Fig. 6A). However, in MCF7/ADR cells, cell cycle arrest at the subG0 phase—which represents cell death—increased (Fig. 6B). The difference in the arrested phase of the cells can be explained by the dual mechanism of DTX according to its concentration (Hernandez-Vargas et al. 2007a, b). DTX induces a transient or prolonged arrest of mitosis at a low or high concentration, respectively (Hernandez-Vargas et al. 2007a, b). Drug-resistant MCF7/ADR cells can continuously efflux DTX out of the cytoplasm, thereby lowering the intracellular DTX concentration. Due to this lowered DTX concentration in MCF7/ADR cells, the prevalence of aberrant mitosis increased due to a relatively short mitosis arrest, which led to an increase the subG0-phase population. Despite differences among the two cell lines, we observed that the apoptosis-inducing mechanism of DTX was consistent with former reports (Kim et al. 2020).

Antitumor efficacy was evaluated by measuring tumor volume and body weight changes after intravenous injections of different drug-loaded formulations. OVCAR3 cells, which are known as MDR cancer cells, were introduced to establish the xenograft mouse model (Vergara et al. 2012; Solomon et al. 2013; Zheng et al. 2018). The DTX-P/R-NLC and CUR-P/R-NLC combination treatment group showed higher antitumor efficacy than other treatment groups, which may be attributed to its high capacity to entrap DTX or CUR. Due to the prolonged circulation and target specificity, co-administration of DTX and CUR using a P/R-NLC system exhibited synergistic therapeutic effects of DTX and CUR. First, as a matrix-type particulate system, NLCs offer several advantages including high DTX or CUR encapsulation, and subsequent sustained release of the cargos (Haider et al. 2020). By encapsulating DTX or CUR in NLCs, these drugs could be protected from labile drug degradation by metabolism and clearance before reaching the target site (Rizwanullah et al. 2021). Due to the high surface-to-volume ratio of NLCs, the pharmacokinetics and biodistribution profiles of the encapsulated drugs could also be improved (Haider et al. 2020). In addition, NLCs may pass through leaky vasculature and accumulate in the surrounding tumor tissue due to enhanced permeability and retention effects owing to their ideal nano-size of approximately 200 nm (Fang et al. 2011; Sanna et al. 2014).

Second, the superior efficacy of the combination of DTX-P/R-NLCs and CUR-P/R-NLCs could be attributed to the enhanced passive and active targeting capability of

P/R-NLCs via surface modification for multifunctionality. For in vivo stability and distribution of nanocarriers, P/R-NLCs had been designed using 1 mol% of hepsin-specific RIPL peptide and 5 mol% PEG3K (Kim et al. 2018). The presence of the PEG moiety on the P/R-NLC surface may reduce mononuclear phagocyte uptake, enhance in vivo stability, and prolong circulation leading to enhanced tumor accumulation by passive targeting (Zhang et al. 2008; Wang et al. 2015a, b). By virtue of the RIPL peptide, P/R-NLCs could specifically bind to hepsin-expressing cancer cells and enhance the simultaneous intracellular delivery of DTX and CUR following their distribution and penetration of tumor tissues (Kim et al. 2020; Kondo et al. 2021). Third, the combination of DTX and CUR also synergistically improved DTX-induced apoptosis in vivo. Although DTX and CUR were encapsulated separately, they were presumed to accumulate simultaneously at the same site of action due to their loading in the same type of P/R-NLC (Dai et al. 2017). In the cytosol of cancer cells, the optimal combination ratio of DTX and CUR would be maintained to trigger an apoptotic cascade by promoting cell cycle arrest in the G2/M phase and enhancing the activation of the apoptosis pathway. Altogether, our results indicate the superior anticancer efficacy of the combination treatment with DTX-P/R-NLCs and CUR-P/R-NLCs against chemoresistant breast cancer.

## Conclusions

A co-administrative system of DTX and CUR using P/R-NLCs was successfully developed with a high DL capacity and an optimized synergistic ratio of DTX-P/R-NLC to CUR-P/R-NLC (1:3, w/w). In both hepsin-expressing MCF7 (drug-sensitive) and MCF7/ADR (drug-resistant) cell lines, the combination showed significantly enhanced cytotoxic and apoptotic effects, owing to enhanced cell cycle arrest in the G2/M or subG0 phase. Further, using an OVCAR3-xenografted mouse model, enhanced in vivo antitumor efficacy of the combination was obtained. Therefore, co-administration of DTX and CUR using P/R-NLCs may be a promising strategy to overcome MDR in cancers. However, for practical development, further clinical studies are required in the future.

## Materials and methods

### Materials

DTX (>99% purity) was kindly gifted by Chong Kun Dang Pharm. Co. (Yongin, Korea). Oleoyl macrogol-6 glycerides (Labrafil® M 1944 CS) and glyceryl distearate (Precirol® ATO 5) were received as gifts from Gattefossé (Saint-Priest, France). CUR (>94% curcuminoid content, >80% curcumin), 3-(4,5-dimethyl-2-thiazolyl)-2,5-diphenyl-2H-tetrazolium bromide (MTT) dye, and phosphate-buffered saline (PBS) tablets were purchased from Sigma–Aldrich Chemical Co. (St. Louis, MO, USA). 1,2-Distearoyl-sn-glycero-3-phosphoethanolamine-N-[maleimide(polyethylene glycol$_{2000}$)] (DSPE-PEG2K-Mal) and 1,2-distearoyl-sn-glycero-3-phosphoethanolamine-*N*-[methoxy(polyethylene glycol$_{3000}$)] (DSPE-PEG3K) were purchased from Avanti Polar Lipids (Alabaster, AL, USA). The RIPL peptide was synthesized by Peptron Co. (Daejeon, Korea). All other chemicals and reagents purchased from commercial sources were of analytical or cell culture grade. PBS (10×, pH 7.4) and cell culture materials, including Roswell Park

Memorial Institute (RPMI) 1640 medium, fetal bovine serum (FBS), penicillin–streptomycin, and trypsin–EDTA (0.25%) were obtained from Invitrogen (Carlsbad, CA, USA). BD Matrigel™ basement membrane matrix was purchased from BD Biosciences (San Jose, CA, USA).

### Cell culture and animals

Human breast adenocarcinoma MCF7 cells and human ovarian adenocarcinoma OVCAR3 cells were purchased from the Korean Cell Line Bank (Seoul, Korea) and multidrug-resistant MCF7 cells (MCF7/ADR) were kindly gifted by Dr. Hwa Jeong Lee (College of Pharmacy, Ewha Womans University, Seoul, Korea). Cells were incubated in RPMI 1640 medium containing antibiotics (100 μg/mL streptomycin and 100 U/mL penicillin G) and 10% (v/v) FBS. Cells were cultured every 2–4 days in a humidified incubator in an atmosphere with 5% $CO_2$ at 37 °C and 95% relative humidity.

Female BALB/c athymic mice ($17 \pm 2$ g, 6 weeks) were purchased from the Hanlim Experimental Animal Laboratory (Gyeonggi-do, Korea). The animal experiments were approved by the Institutional Animal Care and Use Committee of Chung-Ang University, Seoul, Korea (Protocol No. 2020–00072) and carried out in accordance with the National Institute of Health Guidelines for the Care and Use of Laboratory Animals.

### Synthesis of DSPE-PEG2K-RIPL

DSPE-PEG2K-RIPL was synthesized using the thiol-maleimide reaction by conjugating the cysteine residue of the RIPL peptide to DSPE-PEG2K-Mal based on a previous report (Lee et al. 2018). In brief, RIPL peptides were reacted with DSPE-PEG2K-Mal at a molar ratio of 1.12:1 in 2 mL of 0.01 M PBS (pH 7.4) at 25 °C for 48 h with continuous stirring. The resulting mixture was subjected to dialysis for 48 h against distilled water using a dialysis bag (3.5 kDa MWCO, Biotech CE Tubing; Spectrum Laboratories, Inc., Rancho Dominguez, CA, USA) to remove unreacted RIPL peptides and other impurities. The final solution in the dialysis bag was freeze-dried and stored at −20 °C until use.

### Preparation of DTX- or CUR-loaded NLC formulations

DTX- or CUR-loaded P/R-NLCs were prepared using the solvent emulsification–evaporation method (Kim et al. 2020). The compositions of the different NLC samples are summarized in Additional file 1: Table S1. Briefly, the organic phase was prepared by dissolving Labrafil M 1944 CS (liquid oil) and Precirol® ATO 5 (solid lipid) with DTX (4 mg) or CUR (1.6 mg) in dichloromethane (DCM; 0.667 mL). The organic phase was mixed with a 4 mL aqueous solution containing polysorbate 20 (1%, w/v), polyvinyl alcohol (0.5%, w/v), 5 mol% DSPE-PEG3K, and 1 mol% DSPE-PEG2K-RIPL. The mixture was then homogenized at 15,000 rpm for 2 min using an Ultra-Turrax T25 basic disperser (IKA Labortechnik, Staufen, Germany), followed by sonication through a probe-type sonicator (Sonopuls, HD 2070; Bandelin Electronics, Berlin, Germany) operating at 45% power for 3 min under cooling at 4 °C. Finally, the resulting emulsion was evaporated at 25 °C under reduced pressure by magnetically stirring at 300 rpm to withdraw the organic solvent and solidify the NLCs. DTX- or CUR-loaded pNLCs were prepared

using the same procedure, excluding the addition of DSPE-PEG3K and DSPE-PEG2K-RIPL. Empty NLC formulations were prepared without the addition of DTX or CUR. All prepared NLC formulations were maintained at 4 °C and used for the subsequent experiments within 2 weeks. For in vivo intravenous injections, DTX-P/R-NLC and CUR-P/R-NLC solutions were concentrated by centrifugation at 14,000 × *g* for 20 min using Amicon® ultra-centrifugal devices (100 kDa MWCO; Millipore, Billerica, MA, USA). DTX-P/R-NLC and CUR-P/R-NLC residues were diluted with normal saline to reach a concentration of 4 mg/mL and 2.5 mg/mL for DTX and CUR, respectively.

### Preparation of a reference DTX and CUR solution

To mimic a marketed DTX product (Taxotere®), the DTX-Sol was prepared as a reference sample by dissolving DTX at a concentration of 10 mg/mL in normal saline containing polysorbate 80 (25%, w/v) and ethanol (9.75%, v/v) (Guo et al. 2017). To prepare a CUR-Sol, CUR was dissolved in dimethyl sulfoxide (DMSO) at a concentration of 5 mg/mL (Wu et al. 2019). Thereafter, DTX-Sol and CUR-Sol were appropriately diluted with a cell culture medium or normal saline for in vitro and in vivo experiments, respectively. The final concentration of DMSO in the culture was less than 0.2% (nontoxic to cells).

### HPLC analysis of DTX and CUR

Quantitative determination of DTX was performed using an HPLC system consisting of separating modules (Waters® e2695), a UV detector (Waters® e2489), and a data station (Empower® 3), which were purchased from Waters® Corporation (Milford, MA, USA). DTX was separated using a C18 Column (5 μm, $4.6 \times 250$ mm; Shiseido, Tokyo, Japan) with acetonitrile and water (55:45, v/v) as the mobile phase, delivered at a flow rate of 1 mL/min at room temperature. DTX was detected at 230 nm, and the injection volume was 50 μL. The amount of CUR was also quantified using the same HPLC system. Chromatography was carried out on a C18 Column (5 μm, $4.6 \times 250$ mm; Kromasil®, Akzo Nobel, Bohus, Sweden) with acetonitrile and 4% acetic acid (45:55, v/v) as the mobile phase, and delivered at a flow rate of 1 mL/min at 25 °C. CUR was detected at 420 nm, and the injection volume was 50 μL.

### EE and DL

EE and DL of DTX or CUR in DTX- or CUR-loaded NLC formulations were determined as reported earlier: free unencapsulated DTX or CUR were separated using the ultra-filtration method using Amicon® ultra-centrifugal devices (Beloqui et al. 2014). Briefly, DTX- or CUR-loaded NLC samples (500 μL) were centrifuged for 20 min at 14,000 × *g*. The amount of free unencapsulated drug in the filtrate was quantified by HPLC as described above. The following equations were used for the calculations (Ghodrati et al. 2019):

$$EE(\%) = \frac{W_T - W_F}{W_T} \times 100, \tag{1}$$

$$DL(\%) = \frac{W_T - W_F}{W_L} \times 100, \qquad (2)$$

where $W_T$, $W_F$, and $W_L$ represent the total amount of DTX or CUR added, the amount of free DTX or CUR in the filtrate, and the total amount of lipid matrix, respectively.

**Particle size and ZP analysis**

The particle size (diameter, nm), PDI, and ZP of DTX- or CUR-loaded NLCs were determined by dynamic light scattering on a Zetasizer Nano-ZS instrument (Malvern Instruments, Worcestershire, UK). NLC samples were diluted (1:100) in distilled water. All measurements were carried out at 25 °C and each sample was measured in triplicate.

**TEM**

The morphology of DTX- or CUR-loaded NLCs was examined using TEM (Talos L120C; FEI, Czech) at an acceleration voltage of 120 kV. Briefly, NLC samples were diluted tenfold with distilled water and dropped on a carbon-coated grid. The samples were negatively stained with a phosphotungstate solution (2%, w/v) for 1 min. The grid was then washed with double-distilled water, allowed to air-dry at room temperature, and subjected to TEM observation.

**In vitro drug release**

The in vitro release profiles of DTX or CUR from DTX- or CUR-loaded formulations were evaluated using a dialysis bag diffusion method (Rosiere et al. 2018). In prior, considering the concentration of in vitro cell treatment for NLC formulations, DTX-Sol and CUR-Sol were tenfold diluted with PBS. Briefly, diluted DTX-Sol, diluted CUR-Sol, DTX-pNLC, CUR-pNLC, DTX-P/R-NLC, and CUR-P/R-NLC (1 mL each) were placed in a dialysis bag (300 kDa MWCO; Spectrum Laboratories). Then, firmly clipped dialysis bags were completely soaked in PBS (200 mL, pH 7.4), containing 1% (w/v) polysorbate 80, and incubated at 37 °C with magnetic stirring at 100 rpm. At predetermined time points, 1 mL of the release medium was removed and replaced with the equivalent volume of fresh release medium. The concentration of DTX or CUR in the aliquots was analyzed using HPLC as described above. In order to examine the release kinetics of various types of NLCs, results of the release assessment were plotted in various models, such as zero-order, first-order, and Higuchi equations, as follows (Son et al. 2017):

$$Q_t = Q_O - K_O * t, \qquad (3)$$

$$lnQ_t = lnQ_o - K_1 * t, \qquad (4)$$

$$Q_t = K_H * t^{1/2}, \qquad (5)$$

where $Q_t$ is the cumulative amount of drug released at time $t$, $Q_0$ is the initial amount of drug, and t is the time at which the drug release is calculated, and $K_0$, $K_1$, and $K_H$ are release constants of zero-order, first-order, and the Higuchi equations, respectively. The fitting of the data into models was assessed by the determination of the linearity of the plot from the regression factor ($r^2$ value).

**Stability test**

Physical stability of the DTX- or CUR-loaded NLC formulations was determined by monitoring variations in particle size, PDI, and ZP for 4 weeks at $4 \pm 1$ °C (Gupta et al. 2015). To investigate the leakage of DTX or CUR from DTX- or CUR-loaded NLC formulations during storage, changes in EE and DL were monitored using the method described above. Separately, for measuring serum stability, 100 μL of DTX- or CUR-loaded NLC formulations were incubated with 900 μL RPMI1640 cell culture medium containing 20% FBS at 37 °C for up to 48 h. Aliquots were sampled and subjected for the observation of changes in size, PDI, ZP, and DL.

**Combined effects of DTX and CUR**

The combined effects of DTX-P/R-NLCs and CUR-P/R-NLCs at different mass ratios of DTX to CUR (w/w) were assessed against MCF7 and MCF7/ADR cells using the MTT assay. Briefly, MCF7 and MCF7/ADR cells were seeded into 96-well plates at a density of 10,000 cells/well. After incubation for 24 h, the cells were treated with a series of varying concentrations of DTX-P/R-NLCs (0.1–10,000 ng/mL) and CUR-P/R-NLCs (0.3–30,000 ng/mL), or with different combination ratios of DTX-P/R-NLCs and CUR-P/R-NLCs (DTX:CUR = 5:1, 3:1, 1:1, 1:3, and 1:5, w/w). After a 24 h incubation, cells were washed twice with cold PBS and incubated with 100 μL of MTT solution (0.5 mg/mL) for 4 h. The resultant formazan salt crystals were dissolved by adding dimethyl sulfoxide (200 μL) to each well and the absorbance was measured at a wavelength of 450 nm using a microplate reader (Flexstation 3; Molecular Devices LLC, Sunnyvale, CA, USA). The following formula was used to calculate the cell viability (Chen et al. 2018): $\text{Cell viability}(\%) = ([A_T - A_B]/[A_U - A_B]) \times 100$, where $A_T$, $A_B$, and $A_U$ are the absorbance of treated sample, blank control, and untreated sample, respectively. The synergistic effects of different combinations of DTX-P/R-NLCs and CUR-P/R-NLCs were assessed through calculation of the CI using the equation of Chou and Talalay (Chou 2010; Hong et al. 2019). The CI was calculated using the CompuSyn software (Biosoft, Cambridge, UK) with the following equation: $CI = (D)_1/(D_{50})_1 + (D)_2/(D_{50})_2$, where $(D)_1$ and $(D)_2$ represent the $IC_{50}$ values of DTX-P/R-NLCs and CUR-P/R-NLCs in combination, while $(D_{50})_1$ and $(D_{50})_2$ represent $IC_{50}$ values of DTX-P/R-NLCs and CUR-P/R-NLCs alone, respectively. The occurrence of the ratio-dependent synergy was determined by plotting the CI versus the Fa that was calculated as follows: Fa = 1 – (percentage of viability of drug-treated cells / percentage of viability of untreated cells) (Zouaoui et al. 2016).

**Cytotoxicity assessment**

In vitro cytotoxicity levels of DTX-Sol, CUR-Sol, combined DTX-Sol and CUR-Sol (DTX: CUR = 1:3, w/w), DTX-pNLCs, CUR-pNLCs, DTX-P/R-NLCs, CUR-P/R-NLCs, combined DTX-P/R-NLCs and CUR-P/R-NLCs (DTX: CUR = 1:3, w/w), and empty formulations were determined using the MTT assay as described above. Cell viability was measured as the percentage of viable cells relative to the untreated control as described above. All experiments were performed in triplicate, and the results were indicated as means $\pm$ SD. $IC_{50}$ values were determined using GraphPad Prism 7.05 (GraphPad Software Inc., San Diego, CA, USA) via nonlinear regression.

**Cell apoptosis analysis**

Cell apoptosis was assessed using the FITC-annexin V/ apoptosis detection kit with PI (BioLegend, San Diego, CA, UsSA) followed by flow cytometric analysis (FACSCalibur; Becton Dickinson, Franklin Lakes, NJ, USA). Briefly, the MCF7 and MCF7/ADR cells were seeded at a density of $1.5 \times 10^5$ cells/well in 12-well plates and incubated for 24 h to facilitate attachment. The cells were exposed to DTX-loaded formulations and/or CUR-loaded formulations at the DTX-equivalent concentration of 100 ng/mL for 24 h. After incubation, the cells were washed twice with ice-cold PBS, detached with 0.25% trypsin, centrifuged at $1,000 \times g$ for 5 min, washed twice with ice-cold PBS, and resuspended in binding buffer (200 μL). Thereafter, FITC-annexin V (5 μL) and PI (5 μL) were added and mixed for 15 min at room temperature in the dark to stain cells according to the manufacturer's protocol. In total, 10,000 events were counted for each sample using the FL1 and FL2 channels for FITC-annexin V and PI, respectively. Stained untreated cells were used as controls. The data were analyzed using CellQuest Pro software (Becton Dickinson, Franklin Lakes, NJ, USA).

**Cell cycle analysis**

Cell phase distribution was determined based on DNA content using PI and RNAse flow cytometry kits (Abcam, Cambridge, UK), according to the manufacturer's protocol. Briefly, MCF7 and MCF7/ADR cells were seeded at a density of $1.5 \times 10^5$ cells/ well in 12-well plates and allowed to attach for 24 h. Thereafter, cells were treated with DTX-loaded formulations and/or CUR-loaded formulations at the DTX-equivalent concentration of 100 ng/mL for 24 h. Adherent and non-adherent cells were collected via centrifugation at $1000 \times g$ for 5 min and fixed with ice-cold 70% ethanol at $-20$ °C for 4 h. Cells were washed twice with cold PBS to remove any residual ethanol and were collected via centrifugation at $1000 \times g$ for 5 min. Subsequently, cells were resuspended and incubated with PBS (200 μL), consisting of RNase A (550 U/mL) and a PI solution (0.05 μg/mL), to stain the DNA for 30 min at 37 °C. The cell distribution in SubG0, G0/ G1, S, and G2/M phases was measured and analyzed using a flow cytometer using the FL2 channel. The gating was done by distinguishing n and 2n content cells (G0/G1 and G2/M phase, respectively) on the base of DNA content.

**Tumor spheroid growth inhibition assay**

Briefly, MCF7/ADR cells were detached using trypsin–EDTA and passed through a 70 μm cell strainer to generate a single-cell suspension. To prepare 3D spheroids, the MCF7/ADR single-cell suspensions were transferred into 96-well spheroid micro-plates (C.4515; Corning Inc., Kennebunk, ME, USA) at a density of 5000 cells per well. Centrifugation was performed at $126 \times g$ for 5 min to facilitate cellular aggregation in the well. Cell pellets were then incubated for 3 days. The formation of spheroids was monitored using an optical microscope at 100× magnification (KI-400; Optinity, Korea Labtech, Gyeonggi-do, Korea). When the diameter of the spheroids reached approximately 350 μm with uniform size and integrity, the medium was changed to a culture medium containing DTX- or CUR-loaded formulations at the final DTX-equivalent concentration of 500 ng/mL. Culture medium without any formulations was used as

the blank control. Microscopic images were taken every day for 5 days to monitor spheroid growth. To evaluate the inhibition of spheroid growth, the volume ($V$) of the spheroids was measured using the following formula: $V = 0.5 \times D_{max} \times D_{min}^2$, where $D_{max}$ is the maximum diameter and $D_{min}$ is the minimum diameter of each spheroid (Yang et al. 2017a, b). The volume change ratio of a spheroid was calculated using the formula: $N = (V_n/V_0) \times 100\%$, where $V_n$ is the volume of a spheroid at n days after treatment, and $V_0$ is the volume of the spheroid prior to treatment.

### In vivo antitumor efficacy study

The in vivo antitumor effects were investigated in BALB/c nude mice with OVCAR3 cell xenografts. To set up the tumor xenograft model, female BALB/c athymic mice were subcutaneously inoculated with RPMI 1640 medium/Matrigel (100 μL, 50:50 v/v) suspension containing $2 \times 10^6$ OVCAR3 cells in the right flank. Digital calipers (Mitutoyo, Kawasaki, Japan) were used to measure the tumor dimensions. The tumor volume ($\text{mm}^3$) was calculated as (Qu et al. 2014):

$$\text{Tumor volume} = 0.5 \times L \times W^2, \tag{6}$$

where $L$ is length of tumor and W is width of tumor. When tumors reached a volume of 100–110 $\text{mm}^3$, mice were randomly divided into four groups ($n = 4$): (1) DTX-Sol, (2) DTX-NLC, (3) DTX-P/R-NLC, and (4) a combination of DTX-P/R-NLC and CUR-P/R-NLC (DTX:CUR = 1:3, w/w). Each mouse received an intravenous injection via the tail vein at a dose of 5 mg DTX/kg using a 21 G needle for a total of three injections. The first day of administration was designated as day 0. Antitumor efficacy was evaluated weekly for a total of 4 weeks based on the changes in tumor volume and body weights. For further comparison, the percentage of TGI was calculated using the following equation (Liu et al. 2015):

$$\text{TGI}(\%) = (1 - V_t/V_c) \times 100, \tag{7}$$

where $V_t$ and $V_c$ represent the tumor volume of the treated and control groups, respectively, at day 28. General animal health was also recorded to detect potential side effects, including food and water avoidance, impaired movement, and behavioral changes. Median survival time was calculated, and Kaplan–Meier survival curves were plotted using GraphPad Prism (GraphPad Software, San Diego, CA, USA). At the end of the experiment, the mice were sacrificed, and the tumors were excised and photographed.

### Statistical analysis

All values are expressed as the mean $\pm$ standard deviation (SD) ($n \geq 3$). Statistical significance was determined using Student's $t$-test, and differences were considered significant at $p < 0.05$.

### Supplementary information

The online version contains supplementary material available at https://doi.org/10.1186/s12645-022-00119-w.

---

**Additional file 1. Table S1.** Composition of different nanostructured lipid carriers (NLCs) samples. **Fig. S1.** Changes in particle size, polydispersity index (PDI), zeta potential (ZP), and drug loading (DL) capacity in serum-containing RPMI 1640 cell culture medium at 37℃ for 48 h. **Fig. S2.** The effect of co-treatment on the cell viability of MCF7 and

MCF7/ADR cells after 24 h incubation. **Fig. S3.** Cytotoxicity of empty nanostructured lipid carriers (NLCs) on MCF7 and MCF7/ADR cells determined using the MTT assay

## Declarations

### Ethics approval and consent to participate
Not applicable.

### Consent for publication
Not applicable.

### Competing interests
The authors declare that they have no competing interests.

## References
Baek JS, Cho CW (2017) A multifunctional lipid nanoparticle for co-delivery of paclitaxel and curcumin for targeted delivery and enhanced cytotoxicity in multidrug resistant breast cancer cells. Oncotarget 8:30369–30382

Batra H, Pawar S, Bahl D (2019) Curcumin in combination with anti-cancer drugs: a nanomedicine review. Pharmacol Res 139:91–105

Bazak R, Houri M, El Achy S, Kamel S, Refaat T (2015) Cancer active targeting by nanoparticles: a comprehensive review of literature. J Cancer Res Clin Oncol 141:769–784

Beloqui A, Solinis MA, Des Rieux A, Preat V, Rodriguez-Gascon A (2014) Dextran-protamine coated nanostructured lipid carriers as mucus-penetrating nanoparticles for lipophilic drugs. Int J Pharm 468:105–111

Chen D, Pan X, Xie F, Lu Y, Zou H, Yin C, Zhang Y, Gao J (2018) Codelivery of doxorubicin and elacridar to target both liver cancer cells and stem cells by polylactide-co-glycolide/d-alpha-tocopheryl polyethylene glycol 1000 succinate nanoparticles. Int J Nanomed 13:6855–6870

Chou TC (2010) Drug combination studies and their synergy quantification using the Chou-Talalay method. Cancer Res 70:440–446

Dai W, Wang X, Song G, Liu T, He B, Zhang H, Wang X, Zhang Q (2017) Combination antitumor therapy with targeted dual-nanomedicines. Adv Drug Deliv Rev 115:23–45

Fang J, Nakamura H, Maeda H (2011) The EPR effect: Unique features of tumor blood vessels for drug delivery, factors involved, and limitations and augmentation of the effect. Adv Drug Deliv Rev 63:136–151

Ghassami E, Varshosaz J, Jahanian-Najafabadi A, Minaiyan M, Rajabi P, Hayati E (2018) Pharmacokinetics and in vitro/in vivo antitumor efficacy of aptamer-targeted Ecoflex((R)) nanoparticles for docetaxel delivery in ovarian cancer. Int J Nanomed 13:493–504

Ghodrati M, Farahpour MR, Hamishehkar H (2019) Encapsulation of Peppermint essential oil in nanostructured lipid carriers: In-vitro antibacterial activity and accelerative effect on infected wound healing. Colloids Surf A 564:161–169

Guo Y, He W, Yang S, Zhao D, Li Z, Luan Y (2017) Co-delivery of docetaxel and verapamil by reduction-sensitive PEG-PLGA-SS-DTX conjugate micelles to reverse the multi-drug resistance of breast cancer. Colloids Surf B Biointerfaces 151:119–127

Gupta B, Poudel BK, Tran TH, Pradhan R, Cho HJ, Jeong JH, Shin BS, Choi HG, Yong CS, Kim JO (2015) Modulation of pharmacokinetic and cytotoxicity profile of imatinib base by employing optimized nanostructured lipid carriers. Pharm Res 32:2912–2927

Haider M, Abdin SM, Kamal L, Orive G (2020) Nanostructured lipid carriers for delivery of chemotherapeutics: a review. Pharmaceutics 12:288

Hernandez-Vargas H, Palacios J, Moreno-Bueno G (2007a) Telling cells how to die: docetaxel therapy in cancer cell lines. Cell Cycle 6:780–783

Hernandez-Vargas H, Palacios J, Moreno-Bueno G (2007b) Molecular profiling of docetaxel cytotoxicity in breast cancer cells: uncoupling of aberrant mitosis and apoptosis. Oncogene 26:2902–2913

Hong Y, Che S, Hui B, Yang Y, Wang X, Zhang X, Qiang Y, Ma H (2019) Lung cancer therapy using doxorubicin and curcumin combination: targeted prodrug based, pH sensitive nanomedicine. Biomed Pharmacother 112:108614

Imran M, Saleem S, Chaudhuri A, Ali J, Baboota S (2020) Docetaxel: an update on its molecular mechanisms, therapeutic trajectory and nanotechnology in the treatment of breast, lung and prostate cancer. J Drug Deliv Sci Technol 60:101959

Kang MH, Park MJ, Yoo HJ, Hyuk KY, Lee SG, Kim SR, Yeom DW, Kang MJ, Choi YW (2014) RIPL peptide (IPLVVPLRRR RRRRRC)-conjugated liposomes for enhanced intracellular drug delivery to hepsin-expressing cancer cells. Eur J Pharm Biopharm 87:489–499

Kebebe D, Liu Y, Wu Y, Vilakhamxay M, Liu Z, Li J (2018) Tumor-targeting delivery of herb-based drugs with cell-penetrating/tumor-targeting peptide-modified nanocarriers. Int J Nanomedicine 13:1425–1442

Kim CH, Lee SG, Kang MJ, Lee S, Choi YW (2017) Surface modification of lipid-based nanocarriers for cancer cell-specific drug targeting. J Pharm Investig 47:203–227

Kim CH, Sung SW, Lee ES, Kang TH, Yoon HY, Goo YT, Cho HR, Kim DY, Kang MJ, Choi YS, Lee S, Choi YW (2018) Sterically stabilized RIPL peptide-conjugated nanostructured lipid carriers: characterization, cellular uptake, cytotoxicity, and biodistribution. Pharmaceutics 10:199

Kim CH, Kang TH, Kim BD, Lee TH, Yoon HY, Goo YT, Choi YS, Kang MJ, Choi YW (2020) Enhanced docetaxel delivery using sterically stabilized RIPL peptide-conjugated nanostructured lipid carriers: In vitro and in vivo antitumor efficacy against SKOV3 ovarian cancer cells. Int J Pharm 583:119393

Kondo E, Iioka H, Saito K (2021) Tumor-homing peptide and its utility for advanced cancer medicine. Cancer Sci 112:2118–2125

Lee SG, Kim CH, Sung SW, Lee ES, Goh MS, Yoon HY, Kang MJ, Lee S, Choi YW (2018) RIPL peptide-conjugated nanostructured lipid carriers for enhanced intracellular drug delivery to hepsin-expressing cancer cells. Int J Nanomedicine 13:3263–3278

Liang Y, Liu ZY, Wang PY, Li YJ, Wang RR, Xie SY (2021) Nanoplatform-based natural products co-delivery system to surmount cancer multidrug-resistant. J Control Release 336:396–409

Liu K-F, Li C-X, Dai L, Liu J, Wang L-Y, Lei J-D, Guo L-Q (2015) Design, synthesis and in vivo antitumor efficacy of novel eight-arm-polyethylene glycol–pterostilbene prodrugs. RSC Adv 5:51592–51599

Misra R, Sahoo SK (2011) Coformulation of doxorubicin and curcumin in poly(D, L-lactide-co-glycolide) nanoparticles suppresses the development of multidrug resistance in K562 cells. Mol Pharm 8:852–866

Murray S, Briasoulis E, Linardou H, Bafaloukos D, Papadimitriou C (2012) Taxane resistance in breast cancer: mechanisms, predictive biomarkers and circumvention strategies. Cancer Treat Rev 38:890–903

Ojima I, Lichtenthal B, Lee S, Wang C, Wang X (2016) Taxane anticancer agents: a patent perspective. Expert Opin Ther Pat 26:1–20

Patel SS, Acharya A, Ray RS, Agrawal R, Raghuwanshi R, Jain P (2020) Cellular and molecular mechanisms of curcumin in prevention and treatment of disease. Crit Rev Food Sci Nutr 60:887–939

Qi SS, Sun JH, Yu HH, Yu SQ (2017) Co-delivery nanoparticles of anti-cancer drugs for improving chemotherapy efficacy. Drug Deliv 24:1909–1926

Qu MH, Zeng RF, Fang S, Dai QS, Li HP, Long JT (2014) Liposome-based co-delivery of siRNA and docetaxel for the synergistic treatment of lung cancer. Int J Pharm 474:112–122

Rabanel JM, Hildgen P, Banquy X (2014) Assessment of PEG on polymeric particles surface, a key step in drug carrier translation. J Control Release 185:71–87

Rashidi LH, Homayoni H, Chen W (2014) Nanoparticle applications and targeting strategies in cancer diagnosis and treatment. Rev Nanosci Nanotechnol 3:31–51

Ribeiro LN, Franz-Montan M, Breitkreitz MC, Alcantara AC, Castro SR, Guilherme VA, Barbosa RM, De Paula E (2016) Nanostructured lipid carriers as robust systems for topical lidocaine-prilocaine release in dentistry. Eur J Pharm Sci 93:192–202

Rizwanullah M, Ahmad MZ, Garg A, Ahmad J (2021) Advancement in design of nanostructured lipid carriers for cancer targeting and theranostic application. Biochim Biophys Acta Gen Subj 1865:129936

Rosiere R, Van Woensel M, Gelbcke M, Mathieu V, Hecq J, Mathivet T, Vermeersch M, Van Antwerpen P, Amighi K, Wauthoz N (2018) New folate-grafted chitosan derivative to improve delivery of paclitaxel-loaded solid lipid nanoparticles for lung tumor therapy by inhalation. Mol Pharm 15:899–910

Sanna V, Pala N, Sechi M (2014) Targeted therapy using nanotechnology: focus on cancer. Int J Nanomed 9:467–483

Shi C, Zhang Z, Shi J, Wang F, Luan Y (2015) Co-delivery of docetaxel and chloroquine via PEO-PPO-PCL/TPGS micelles for overcoming multidrug resistance. Int J Pharm 495:932–939

Shrestha S, Wu J, Sah B, Vanasse A, Cooper LN, Ma L, Li G, Zheng H, Chen W, Antosh MP (2019) X-ray induced photodynamic therapy with copper-cysteamine nanoparticles in mice tumors. Proc Natl Acad Sci U S A 116:16823–16828

Solomon MA, Shah AA, D'souza GG (2013) In Vitro assessment of the utility of stearyl triphenyl phosphonium modified liposomes in overcoming the resistance of ovarian carcinoma Ovcar-3 cells to paclitaxel. Mitochondrion 13:464–472

Son G-H, Lee B-J, Cho C-W (2017) Mechanisms of drug release from advanced drug formulations such as polymeric-based drug-delivery systems and lipid nanoparticles. J Pharm Investig 47:287–296

Sun Y, Hu H, Jing X, Meng Q, Yu B, Cong H, Shen Y (2021) Co-delivery of chemotherapeutic drugs and cell cycle regulatory agents using nanocarriers for cancer therapy. Sci China Mater 64:1827–1848

Vergara D, Bellomo C, Zhang X, Vergaro V, Tinelli A, Lorusso V, Rinaldi R, Lvov YM, Leporatti S, Maffia M (2012) Lapatinib/ Paclitaxel polyelectrolyte nanocapsules for overcoming multidrug resistance in ovarian cancer. Nanomedicine 8:891–899

Wang L, Luo Q, Lin T, Li R, Zhu T, Zhou K, Ji Z, Song J, Jia B, Zhang C, Chen W, Zhu G (2015a) PEGylated nanostructured lipid carriers (PEG-NLC) as a novel drug delivery system for biochanin A. Drug Dev Ind Pharm 41:1204–1212

Wang S, Qiu J, Shi Z, Wang Y, Chen M (2015b) Nanoscale drug delivery for taxanes based on the mechanism of multidrug resistance of cancer. Biotechnol Adv 33:224–241

Wei Y, Pu X, Zhao L (2017) Preclinical studies for the combination of paclitaxel and curcumin in cancer therapy (Review). Oncol Rep 37:3159–3166

Wu W, Wu J, Fu Q, Jin C, Guo F, Yan Q, Yang Q, Wu D, Yang Y, Yang G (2019) Elaboration and characterization of curcumin-loaded Tri-CL-mPEG three-arm copolymeric nanoparticles by a microchannel technology. Int J Nanomedicine 14:4683–4695

Xu S, Jin Z, Zhang Z, Huang W, Shen Y, Wang Z, Guo S (2019) Precise ratiometric co-loading, co-delivery and intracellular co-release of paclitaxel and curcumin by aid of their conjugation to the same gold nanorods to exert synergistic effects on MCF-7/ADR cells. J Drug Deliv Sci Technol 54:101383

Yang Z, Sun N, Cheng R, Zhao C, Liu J, Tian Z (2017a) Hybrid nanoparticles coated with hyaluronic acid lipoid for targeted co-delivery of paclitaxel and curcumin to synergistically eliminate breast cancer stem cells. J Mater Chem B 5:6762–6775

Yang Z, Sun N, Cheng R, Zhao C, Liu Z, Li X, Liu J, Tian Z (2017b) pH multistage responsive micellar system with charge-switch and PEG layer detachment for co-delivery of paclitaxel and curcumin to synergistically eliminate breast cancer stem cells. Biomaterials 147:53–67

Zhang X, Gan Y, Gan L, Nie S, Pan W (2008) PEGylated nanostructured lipid carriers loaded with 10-hydroxycamptothecin: an efficient carrier with enhanced anti-tumour effects against lung cancer. J Pharm Pharmacol 60:1077–1087

Zhang RX, Wong HL, Xue HY, Eoh JY, Wu XY (2016) Nanomedicine of synergistic drug combinations for cancer therapy - Strategies and perspectives. J Control Release 240:489–503

Zheng X, Andruska N, Lambrecht MJ, He S, Parissenti A, Hergenrother PJ, Nelson ER, Shapiro DJ (2018) Targeting multidrug-resistant ovarian cancer through estrogen receptor α dependent ATP depletion caused by hyperactivation of the unfolded protein response. Oncotarget 9:14741–14753

Zouaoui N, Mallebrera B, Berrada H, Abid-Essefi S, Bacha H, Ruiz MJ (2016) Cytotoxic effects induced by patulin, sterigmatocystin and beauvericin on CHO-K1 cells. Food Chem Toxicol 89:92–103

## Publisher's Note